Applied Catalysis B: Environmental 338 (2023) 123076

Contents lists available at ScienceDirect

Applied Catalysis B: Environmental

journal homepage: www.elsevier.com/locate/apcatb

Superior performance of catalytic ozonation on molecular-level transformation of effluent organic matter and self-cleaning property in catalytic ozonation membrane reactor

Chen Li [a], Zhenbei Wang [a], Ao Li [b], Zilong Song [c], Ruijun Ren [a], Kuichang Zuo [d,e], Fei Qi [a,*], Amir Ikhlaq [f], Oksana Ismailova [g,h]

[a] Beijing Key Lab for Source Control Technology of Water Pollution, College of Environmental Science and Engineering, Beijing Forestry University, Beijing 100083, China
[b] China Urban Water Association, Courtyard 48, Beiwa Road, Haidian District, Beijing 100048, China
[c] College of Environmental Science and Engineering, Sun Yat-Sen University, Guangzhou 510275, China
[d] College of Environment Sciences and Engineering, Peking University, Beijing 100871, China
[e] The Key Laboratory of Water and Sediment Sciences, Ministry of Education, Peking University, Beijing 100871, China
[f] Institute of Environment Engineering and Research, University of Engineering and Technology, GT Road, 54890 Lahore, Punjab, Pakistan
[g] Uzbekistan-Japan Innovation Center of Youth, Tashkent, Uzbekistan
[h] Turin Polytechnic University, Tashkent, Uzbekistan

ARTICLE INFO

Keywords:
Catalytic ozonation membrane reactor
Effluent organic matter
Self-cleaning
Membrane fouling
FT-ICR MS

ABSTRACT

Catalytic ozonation membrane reactor (COMR) is one of the most promising technologies for municipal wastewater reclamation. Herein, we evaluated superior performance of catalytic ozonation in COMR through filtration of effluent organic matter (EfOM) using the origin and three catalytic membranes. We found that filtration primarily contributed to rejection of protein-like fluorescence enriched in relatively high-oxygen compounds (O/C >0.4) with high molecular weight and catalytic ozonation further removed humic-like materials and highly unsaturated, aromatic and reduced compounds (O/C<0.4; H/C<1.3), demonstrating complementary function of catalytic ozonation and filtration. The superior performance of catalytic ozonation than ozonation is reflected in higher removal of medium molecular weighted humic-like materials and S-containing compounds, enhancing the mineralization and reaction extent of EfOM. Additionally, catalytic ozonation exhibited strong self-cleaning property and eliminated irreversible membrane fouling. Our findings provide molecular-level insights into the reaction mechanism governing the COMR towards municipal wastewater reclamation.

1. Introduction

Due to global water scarcity, municipal wastewater reclamation has gained increasing attention and application [1]. Effluent organic matter (EfOM) composed of dissolved organic matter (DOM) and emerging contaminants present in biologically treated secondary effluent pose a significant threat for ecological system and human health during water reuse [2,3]. Catalytic membrane-based oxidation-filtration coupling of membrane separation and advanced oxidation processes (AOPs) has gained increasing attention in recent years for advanced water treatment due to its effective removal of organic contaminants, self-cleaning and process intensification [4]. Catalytic ozonation membrane reactor (COMR) is probably the most promising for commercial wastewater reclamation treatment, considering appealing merits such as flexible reactor design, mild reaction conditions, fast oxidation and environmental-friendly and no secondary pollution [5,6].

Fe_2O_3 [7], MnO_2 [8], TiO_2 [9], CeO_x [10], $CuMn_2O_4$ [11], rGO [12], and g-C_3N_4 [13] are commonly investigated catalysts for catalytic membrane fabrication in COMR to increase the production of hydroxyls radicals, and increase the degradation performance. In our previous study, $CuMn_2O_4$/rGO [12] and $CuMn_2O_4$/g-C_3N_4 [14] catalytic membranes-based ozonation-filtration have showed excellent performance on degradation of a micro-pollutant of concern. Ceramic ultrafiltration membranes commonly involved in oxidation-filtration system retain compounds with larger particle size, and at the same time ozone could offer complementary functions of degradation of micro-pollutant

* Corresponding author.
E-mail address: qifei@bjfu.edu.cn (F. Qi).

https://doi.org/10.1016/j.apcatb.2023.123076
Received 23 April 2023; Received in revised form 10 June 2023; Accepted 6 July 2023
Available online 7 July 2023

and other small organic molecules [15]. While the results of current studies focusing on removal of single pollutant are encouraging [16–18], there remains a need to better understand transformation of complex EfOM in real water samples during ozonation process. Moderate mineralization of EfOM and ozonation by-products have been observed during ozonation [3,19,20]. However, the oxidation by-products and refractory organics may not be retained by the membrane separation, and thus still remain in the membrane effluent, which might form disinfection by-products in the downstream process [21,22]. Thus, the ability of oxidation and membrane separation needs to be designed for optimal matching in the studies of oxidation-filtration. Without understanding the residual EfOM in the membrane effluent after ozonation-filtration process, it is difficult to treat the secondary effluent more effectively and assess the environmental risk related with the discharge of reclaimed water into the environment.

Catalytic ozonation is expected to show better degradation efficiency than ozonation [23,24], but their respective reactivity with EfOM composition is largely unknown [25]. Previous studies have investigated the evolution of EfOM during ozonation and have identified the selectivity of ozonation towards different constituents and functional groups of EfOM using conventional spectrographic and chromatographic tools [20,26,27]. With advances in high resolution mass spectrometry, molecular-level composition data for mixed organic matters will be gained to improve our understanding of organic matter chemistry [28,29]. Currently, increasing studies have employed fourier transform ion cyclotron resonance mass spectrometry (FT-ICR MS) to characterize the molecular transformation of EfOM during AOPs [30–32]. Phungsai, et al. [33] found that the unsaturated CHO molecules were preferentially removed in municipal wastewater during ozonation and produced relatively more saturated compounds. Song, et al. [34] reported that humic acid-like substances blocking membrane pores were preferentially removed in N-doped reduced graphene oxide (N-rGO)-tailored CM with ozone. Zhang, et al. [35] unveiled that transformation of EfOM by the oxygenation reaction (+3 O) and decyclopropyl ($-C_3H_4$)) occurred during ozonation of municipal secondary effluent. The role of adsorption, electro-sorption, and oxidation in molecular-level removal of EfOM in electrochemical CM has also been elucidated [36]. However, limited studies are available concerning the molecular transformation of EfOM during (catalytic) ozonation-filtration for real municipal wastewater reuse. Additional advantage of catalytic membrane-based oxidation-filtration is self-cleaning of membrane fouling. The EfOM constituents impacts membrane fouling behaviors [27]. Thus, unravelling molecular transformation of EfOM could also contribute to elucidating the self-cleaning mechanism.

In this study, we prepared three kinds of catalytic ceramic membranes, namely $CuMn_2O_4$ ceramic membrane (CMO/CM), g-C_3N_4 ceramic membrane (CN/CM) and $CuMn_2O_4$/g-C_3N_4 ceramic membrane (CMO/CN/CM) and compared the performance of catalytic membranes with the origin ceramic membrane in COMR for treatment of municipal secondary effluent. We first characterized EfOM by fluorescence excitation-emission matrices (EEMs) coupled with parallel factor analysis (PARAFAC), synchronous fluorescence (SF) coupled with two-dimensional correlation spectroscopy (2D-COS) and molecular weight (MW) distribution. We further unraveled the molecular transformation of EfOM using FT-ICR MS analysis and characterized the fouled membrane surfaces and foulants. We then corelated the EfOM properties to fouling resistance and elucidated the self-cleaning mechanism.

2. Materials and methods

2.1. Materials and reagents

The tubular γ-Al_2O_3-ZrO_2 ceramic ultrafiltration membranes with mean pore size of 50 nm (Nanjing AIYUQI Membrane Technology Co., Ltd, Nanjing, China) were used in this study. The total filtration area of CM is 0.0133 m^2 with 19 channels in 70 mm length. Water samples used in this study were collected from the secondary effluent of a wastewater treatment plant in Beijing, China and stored at 4 ℃. The quality of secondary effluent is shown in Table S1. The initial pH of the secondary effluent from a municipal wastewater treatment plant is 7.06.

2.2. Fabrication of catalysts and catalytic ceramic membranes

In this study, $CuMn_2O_4$, g-C_3N_4 and $CuMn_2O_4$/g-C_3N_4, was loaded on the origin ceramic membrane to fabricate catalytic membrane via a facile filtration–deposition process which has been reported in our previous study [12]. The obtained origin and catalytic membranes were defined as CM, CMO/CM, CN/CM and CMO/CN/CM. The detailed process of catalysts and catalytic ceramic membranes preparation were described in Text S1.

2.3. Catalytic ozonation membrane reactor set up and operation procedure

Fig. 1 showed the catalytic ozonation membrane reactor (COMR) set up in this study including an ozone injection system and membrane module. Ozone was produced by a standard laboratory ozone generator (3S-A5, Beijing Tonglin Gaoke Technology, Beijing, China) with high purity oxygen as a gas source and then pumped to a stainless-steel water tank containing test solution (1.2 L). A peristaltic pump (UIP, Beijing, China) was used to inject the feed water into the membrane device (TOPS-3070B, Beijing, China) and the concentrate was recycled to the reactor. The transmembrane pressure (TMP) was constant at 0.2 bar monitored by a pressure sensor (TOPS/CM-M000, Beijing, China). The permeate flux (J) was monitored using an electronic balance (FR4202CN, Beijing, China). Membrane filtration tests by the origin CM and catalytic CMs were defined as CM-F, CMO/CM-F, CN/CM-F and CMO/CN/CM-F. Ozonation-filtration tests using the origin CM and catalytic CMs were defined as CM-O-F, CMO/CM-O-F, CN/CM-O-F and CMO/CN/CM-O-F. Ozone dosage was selected as 10 mg/L and 20 mg/L in the gas stream. Membrane filtration was operated in a cross-flow mode for 30 min. Physical and chemical cleaning experiments were performed after four consecutive cycles of filtration, in which the feed water was changed. Physical cleaning was performed using deionized water under the flow rate of 100 mL/min and chemical cleaning was through immersed in NaOH solution (0.02 M) under 85 ℃ for 2 h.

2.4. Water quality analysis

Chemical oxygen demand (COD) of secondary effluent was measured using a WTW COD kit (10–150 mg/L, WTW, Germany) and UV–visible absorbance was recorded by a spectrophotometer (UV2600, TECH COMP, China). EEM fluorescence spectra and SF fluorescence spectra were recorded using a spectrophotometer (F-7000, Hitachi, Japan). The MW distribution was obtained using a high-performance liquid chromatography-gel chromatography (Waters 2695, USA) with an UV detector at 254 nm. The concentration of •OH and $\bullet O_2^-$ was quantitatively determined using a fluorescence spectrometer (F-7000, Hitachi, Japan). Other analytical methods and detailed procedures are described in Text S2.

2.5. FT-ICR-MS analysis

An FT-ICR-MS (Bruker, German) equipped with a 9.4 T superconducting magnet and an electrospray ionization (ESI) source was used to analyze the EfOM composition at molecular level. All samples were pretreated by solid phase extraction (SPE) cartridges to remove salt. Mass spectrometers were externally calibrated using sodium formate solution and internally recalibrated using known homologous series of EfOM samples. And the detailed sample extraction and FT-ICR-MS condition are described in Text S3 followed by Geng, et al. [37].

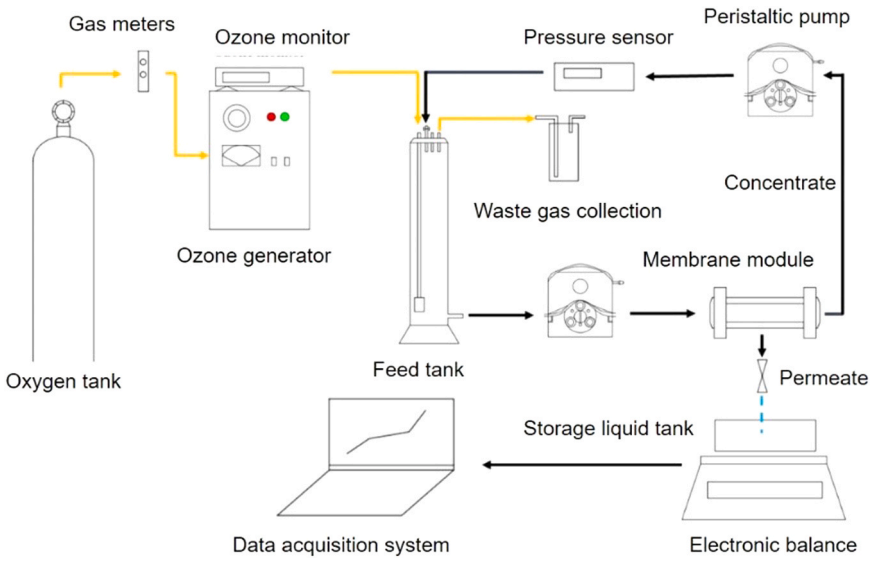

Fig. 1. Schematic of COMR used in this study.

2.6. Fouled membrane characterization

Clean and fouled membrane surface were characterized by Contact Angle Measuring Instrument (JC2000), SEM (Merlin, Zeiss, German), and Atomic Force Microscopy (AFM) (Multimode 8, Bruker, German). Detailed procedures are available in Text S4.

2.7. Data processing

The SF spectra obtained by different experiments were used to obtain the 2D-COS maps with the software 2Dshige released by KwanseiGakuin University, Japan to reveal the sequential order of DOM fluorescence variation [38]. EEM-PARAFAC modeling was performed in MATLAB 2010a (Mathworks, USA) with the DOMFluor Toolbox based on the tutorial of Stedmon and Bro [39]. A series of PARAFAC models between 3 and 7 components were generated. Split-half analysis and random initialization were used to validate the identified model components. The maximum fluorescence intensity (F_{max}) of the identified components was utilized to represent the relative amounts of the individual EfOM component.

The van Krevelen (VK) diagram is used for visualizing the FT-ICR MS data, by plotting molecular H/C ratio as a function of molecular O/C ratio. The VK diagram is divided into seven regions, corresponding to seven compound classes, as shown in Table S2 [40,41]. The FT-ICR MS spectra were also divided into three molecular size groups, i. e., high Mw ($>$ 400 m/z), medium Mw (300–400 m/z), and low Mw ($<$ 300 m/z) fractions. H/C, O/C, double bond equivalent (DBE), modified aromaticity index (AI_{mod}), nominal oxidation state of carbon (NOSC) and relative abundance (R_i) were calculated based on FT-ICR-MS data. AI_{mod} and DBE were used to evaluate the aromaticity and unsaturation of compounds. The NOSC was used to reflect the redox potential of a given formula. More descriptions about these parameters are available in Text S5. The Bray-Curtis analysis based on the relative FT-ICR-MS peak intensities was performed to reveal the statistical dissimilarity of EfOM in COMR.

3. Results and discussion

3.1. Transformation and removal of EfOM in COMR by fluorescence spectroscopy

We first fabricated three kinds of catalytic CMs (Text S1) and found that they maintain relatively high-water flux (Fig. S1). Pure water flux of the origin CM, CMO/CM, CN-CM and CMO/CN/CM were 259.6 $\pm$ 18.8 L/m^2/h, 259.7 $\pm$ 2.6 L/m^2/h, 227.9 $\pm$ 2.5 L/m^2/h and 261.3 $\pm$ 18.8 L/m^2/h, respectively. We then evaluated EfOM removal performance in COMR by spectrographic and chromatographic methods. The removal of EfOM as COD and UV_{254} was very limited by membrane separation (Fig. 2), and only large-sized organics (>10000 Da) removal was observed (Fig. S2). When combined with O_3 (10.0 mg/L), the UV_{254} removal efficiencies were increased to 39.8%, 61.9%, 58.3% and 56.6%, and COD removal efficiencies were increased to 27.8%, 30.6%, 19.4% and 25.0% for CM, CMO/CM, CN/CM, and CMO/CN/CM, respectively (Fig. 2). And increasing O_3 dosage increased removal efficiencies of UV_{254} and COD. EfOM removal increased in COMR because (catalytic) ozonation further degraded small-sized (100–1000 Da) and middle-sized (1000–10000 Da) molecules (Fig. S2; details in Table 1) by ozonation or interface catalytic ozonation [42]. We confirmed limited COD removal of EfOM during ozonation-filtration process. We found that catalytic CMs presented stronger organic removal performance compared to the origin CM in COMR (Fig. 2). But for CN/CM, the lower COD removal than the origin CM was explained by the release of C_3N_4 into the membrane permeate. The stability of C_3N_4 coating on membrane surface is a major concern.

PARAFAC model output showed that four fluorescent components were identified (Fig. S3). C1 exhibited major peaks at 240/350 nm (Ex/Em), implying the presence of tryptophan-like or protein-like component; C2 exhibited primary and secondary maxima at 240/394 nm (Ex/Em) and 315/394 nm (Ex/Em), respectively, which are assigned to microbial humic-like component; C3 exhibited primary and secondary maxima at 225/340 nm (Ex/Em) and 275/340 nm (Ex/Em), respectively, which are assigned to protein-like component; C4 exhibited primary and secondary maxima at 265/430 nm (Ex/Em) and 360/430 nm (Ex/Em), respectively, which are assigned to terrestrial humic-like component [21]. The origin CM showed only 7.45% and 21.74% removal of C1 and C3 by membrane separation and the three catalytic CMs showed increased removal efficiencies of four fluorescent components (Fig. 3A), in which the highest rejection efficiency of C3 primarily contributed to the membrane fouling [43]. After adding O_3, the removal of four components were further increased, especially for C2 and C4, because the electrophilicity of O_3 favors their reaction with aromatic compounds in humic-acids.[44] In addition, catalytic ozonation-filtration led to much higher removal of C2 compared to ozonation-filtration. Higher removal efficiency showed by catalytic CMs is due to the non-selective attack of·OH derived from catalytic ozone decomposition. 90.05% removal of C1, 95.64% removal of C2, 89.79%

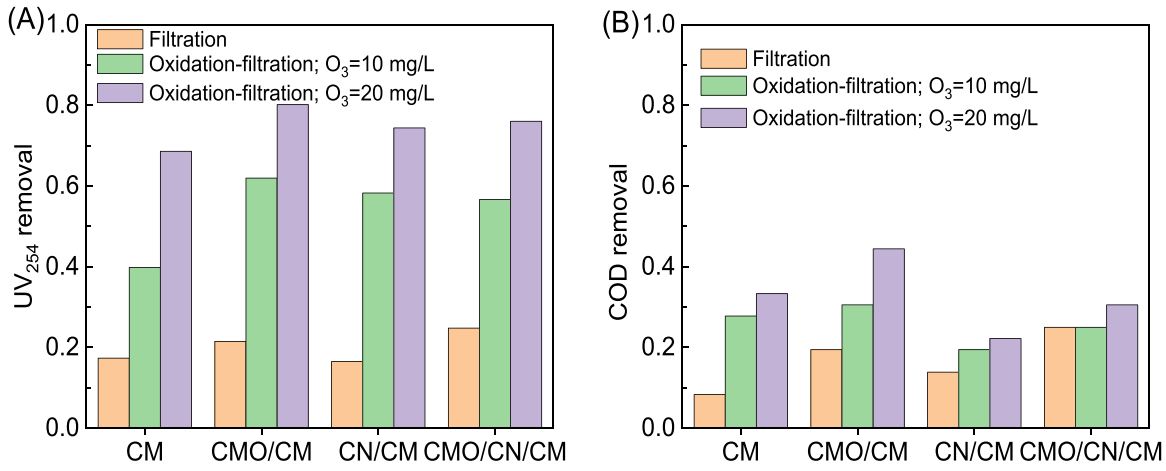

Fig. 2. The removal of EfOM as UV_{254} (A) and COD (B) during filtration and (catalytic) ozonation-filtration for CM, CMO/CM, CN/CM, and CMO/CN/CM.

Table 1
The removal of EfOM after filtration and COMR based on molecular weight distribution.

	Filtration (%)			COMR (10 mg/L O_3) (%)			COMR (20 mg/L O_3) (%)		
	100–1000 Da	1000–10000 Da	> 10000 Da	100–1000 Da	1000–10000 Da	> 10000 Da	100–1000 Da	1000–10000 Da	> 10000 Da
CM	0	0	83.3	64.4	57.3	93.1	79.4	69.8	100.0
CMO/CM	0	8.6	100.0	33.8	66.3	100.0	78.2	70.9	100.0
CN/CM	0	3.3	100.0	29.2	35.8	73.4	71.7	67.4	88.0
CMO/ CN/CM	0	19.2	100.0	78.5	58.2	100.0	48.8	70.1	100.0

removal of C3, and 85.58% removal of C4 in the presence of O_3 (10 mg/L) for CMO/CM were presented in Fig. 3A. CMO/CM showed the best fluorescent degradation efficiency among three catalytic CMs. We also found that a prominent peak in the region of Ex/Em: 220–260 nm/300–400 nm for CN/CM and CMO/CN/CM, albeit with weaker intensity for CMO/CN/CM (Fig.S4(A-D)). Interestingly, similar peak patterns were also observed in the EEM analysis of g-C_3N_4 (as shown in Fig.S4E), specifically in the region of Ex/Em: 220–260 nm/300–400 nm. The phenomenon of g-C_3N_4 release can be attributed to the weak binding ability between the g-C_3N_4 catalyst and the surface of the ceramic membrane. Factors such as the shear force of the water flow and the friction generated by ozone bubbles contribute to the flow of g-C_3N_4 into the effluent. However, we observed that the loss of $CuMn_2O_4$/g-C_3N_4 catalyst was mitigated, suggesting that the combination of $CuMn_2O_4$ and g-C_3N_4 strengthens the binding ability between the catalyst and the ceramic membrane.

Synchronous fluorescence (SF) spectrum in Fig. S5(A-C) showed peaks at 276 nm, 338 nm and 380 nm, which were ascribed to protein-like, fulvic-like and humic-like substances, respectively [45]. We obtained pseudo-first order kinetic constants (k_{obs}) and degradation order of EfOM components based on SF spectrum. The k_{obs} of protein-like, fulvic-acid-like and humic acid-like materials were 0.251, 0.258 and 0.342 min^{-1}, for the origin CM, and were 0.265, 0.247 and 0.349 min^{-1} for the CMO/CM in the presence of O_3 (10 mg/L) (Table 2). When O_3 dosage was further increased to 20 mg/L, the degradation efficiency of fulvic-like and humic-like substances increased significantly. We have also the quantified the amount of •OH and $•O_2^-$ in COMR. As illustrated in the Fig. S6, our results demonstrate that the catalytic process enhances the generation of •OH and $•O_2^-$, with the concentration of •OH being higher than that of $•O_2^-$. Among the three catalytic membranes compared, CMO/CN/CM exhibited a slightly higher •OH concentration than CMO/CM and CN/CM, while the $•O_2^-$ concentration remained similar. Thus, the catalytic ozonation further enhanced the reaction rate and CMO/CM and CMO/CN/CM presented strong degradation performance.

2D-COS was further utilized to analyze SF spectra to reveal the sequential order of EfOM fluorescence variation during (catalytic) ozonation-filtration. We analyzed the synchronous (Fig. S7) and asynchronous maps (Fig. 3(B-D)) of samples obtained after filtration by CMO/CM, ozonation-filtration by CM and catalytic ozonation-filtration by CMO/CM with O_3 dosage of 20 mg/L. The positively signed auto-peak at 276/276 nm suggested the preferential removal of the protein-like materials by membrane filtration (Fig. S7A and Fig. 3B). The auto-peak located at 276/276 nm, 338/338 nm and 380/380 nm with red colors in asynchronous maps (Fig. S7(B and C)) suggested that the degradation of protein-like, fulvic-acid-like and humic-acid-like materials occurred predominantly during (catalytic) ozonation-filtration and no internal conversion occurred. According to the intensities of the main auto-peaks, the treatment that caused the fluorescence change would be in the order of catalytic ozonation-filtration > ozonation-filtration > filtration. In asynchronous map of ozonation-filtration (Fig. 3C), two cross-peaks were centered at 338/276 nm with red colors, and three cross-peaks were centered at 276/270 nm, 380/338 nm and 380/270 nm with blue color. Therefore, the sequential degradation of EfOM during ozonation-filtration occurred in the order of 270 nm (protein-like) →338 nm (fulvic-like) → 380 nm (humic-like). But there were two cross-peaks at 338/276 nm and 380/276 nm with red colors and one major cross-peak at 380/338 nm with blue color in Fig. 3D. Thus, catalytic ozonation-filtration resulted in different sequential order of 338 nm (fulvic-like) → 380 nm (humic-like) → 276 nm (protein-like).

We conclude that membrane separation contributes to removal of larger protein-like substances (>10000 Da) and COMR treatment further remove fulvic-like and humic-like substances in the range of 100–1000 Da and 1000–10000 Da. In addition, catalytic ozonation could preferential remove middle-sized microbial humic-like materials, and increase the reaction rate compared to ozonation. The sequential degradation order of EfOM differs between ozonation- and catalytic ozonation- filtration. The fulvic-like acids that are easy to block the membrane pores were preferably removed for catalytic ozonation.

In comparison to the three CMs investigated, we have confirmed the release of g-C_3N_4 into the membrane permeates for CN/CM. Consequently, ensuring the stability of the g-C_3N_4 coating on the membrane

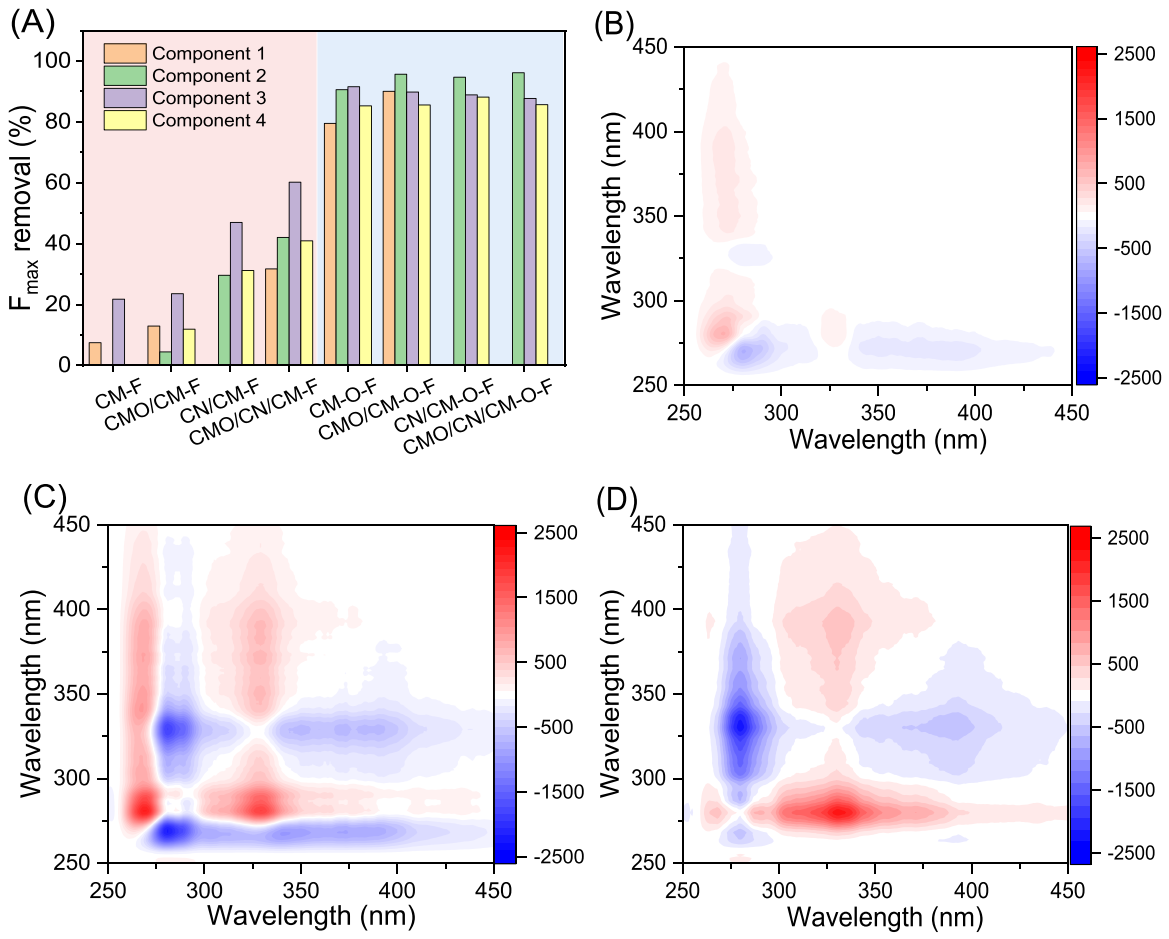

Fig. 3. EfOM degradation efficiency according to the EEM-PARAFAC output (A) and 2D-COS of asynchronous fluorescence spectra during filtration for CMO/CM (B), ozonation-filtration for CM (C) and catalytic ozonation-filtration for CMO/CM in the presence of 20 mg/L O_3 (D).

Table 2
The pseudo-first order kinetic constant (k_{obs}) of protein-like, fulvic-like and humic-like materials calculated based on synchronous fluorescence spectra.

	Filtration			[Ozone] = 10 mg/L			[Ozone] = 20 mg/L		
Substances	Protein-like	Fulvic-like	Humic-like	Protein-like	Fulvic-like	Humic -like	Protein-like	Fulvic-like	Humic-like
k_{obs} (min^{-1})	k_1	k_1	k_1	k_1	k_1	k_1	k_1	k_1	k_1
CM	0.037	0.001	0.027	0.251	0.258	0.342	0.269	0.440	0.438
CMO/CM	0.083	0.000	0.048	0.265	0.247	0.349	0.270	0.450	0.457
CN/CM	0.125	0.058	0.082	0.223	0.368	0.233	0.313	0.416	0.413
CMO/CN/CM	0.132	0.089	0.121	0.248	0.383	0.226	0.271	0.463	0.463

surface emerges as a significant concern. Additionally, $CuMn_2O_4$ and $CuMn_2O_4$/g-C_3N_4 exhibited similar efficiency in the degradation of EfOM. Considering the economic feasibility, it is noteworthy that CMO/CM proves to be a more suitable choice for application in COMRs for wastewater reclamation.

3.2. *The superior performance of catalytic ozonation than ozonation in molecular-level*

We revealed changes in molecular composition of EfOM in COMR using FT-ICR MS. The EfOM in secondary effluent were mostly distributed within the MW of 200–600 *m/z* (as presented in Fig. S8). The intensity of peak presented no obvious change after the origin CM filtration while the compounds with higher M_W of 400–600 *m/z* diminished significantly after catalytic CM filtration. Thus, the catalytic CMs increased the rejection of larger compounds through enhanced steric effect, which was coincident with the removal efficiencies of UV_{254} and COD during filtration in Fig. 2. After adding O_3, the intensity of peak within the M_W of 200–600 *m/z* decreased significantly for various CMs. The compounds with high $m/z > 400$ and low M_W $m/z < 300$ almost diminished after catalytic ozonation-filtration.

The relative abundance of major elemental formulas classified as CHO, CHON, CHOS and CHONS in raw secondary effluent and in treated water by filtration and COMR was analyzed in VK plot, as described in Fig. S (9–17). The distribution of R_i of major compound classes after filtration and after COMR treatment was presented in Fig. 4. We observed that the distribution of formula classes was CHO (65.9%), CHON (25.02%), CHOS (7.57%), and CHONS (1.51%) and the distribution of the major compound classes in CHO, CHON, CHOS and CHONS were lignin (66.60%), protein (13.39%), lipid (10.84%), unsaturated hydrocarbon (8.65%), tannin (0.18%), aromatic structure (0.17%), and carbohydrate (0.14%) in the raw secondary effluent. Lignin compounds mainly consisted of polyphenolic oligomers or the degradation products of carboxylic acids and alicyclic compounds [46].

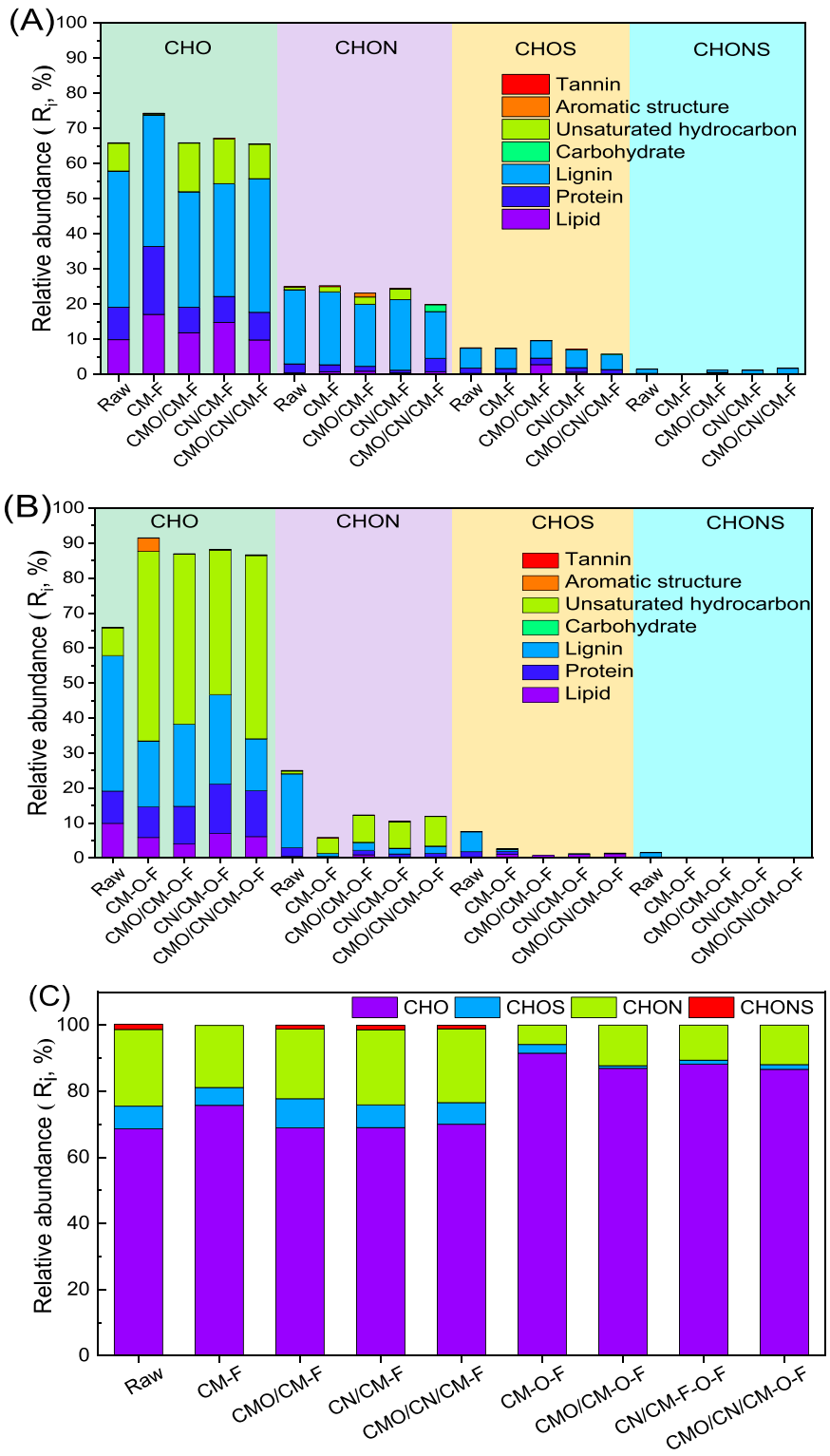

Fig. 4. The relative abundance (R_i) of different formula classes (CHO, CHON, CHOS and CHONS) and distribution of the major compound classes of treated water after filtration (A) and after (catalytic) ozonation-filtration in the presence of 20 mg/L O_3 (B). Relative abundance of CHO, CHON, CHOS and CHONS (C).

The retention of CHO, CHON, CHOS and CHONS by filtration alone is very limited (Fig. 4A). After adding O_3, R_i of CHO increased; but R_i of CHON, CHOS and CHONS decreased significantly compared to filtration (Fig. 4B). Thus, CHON, CHOS and CHONS were transformed to CHO during COMR treatment through oxidative desulfurization and oxidative denitrification. R_i of CHO were lower but that of CHON, CHOS and CHONS were higher for catalytic CMs than that for the origin CM (Fig. 4C). This difference was because more CHO compounds were mineralized into CO_2 by catalytic ozonation than ozonation. CHONS compounds were completely removed in COMR. And ozonation-filtration led to higher CHON removal but lower CHOS removal than catalytic ozonation-filtration. With regard to the major compound classes, we observed that R_i of unsaturated hydrocarbon in CHO and CHON formula increased, R_i of lignin and protein in CHON

formula were degraded and major compounds in CHOS formula were 100% removed except some lipid compounds. This might be due to the decomposition of the large unsaturated organic compounds into small amino sugar compounds under catalytic ozonation [47]. It has been reported that O_3 reacted with polycyclic aromatics and polyphenols to produce more biodegradable intermediates such as phenolic and lipids [48]. We also observed that relative intensity and chemical diversity of EfOM showed similar change patterns among various catalytic CMs during COMR treatment.

We further applied additional index to complement the VK plot, as illustrated in Table S3. Membrane separation decreased the value of O/C but (catalytic) ozonation-filtration increased it. The lower value of O/C after separation could be ascribed to the preferential retention of oxygen-containing compounds. The average O/C was recorded as 0.35, 0.38, 0.40, 0.39 and 0.46 for raw water and filtrated water by CM, CMO/CM, CN/CM, and CMO/CN/CM in the presence of O_3, respectively. The higher value of O/C could be ascribed to the dominant oxygenation reaction (+3 O) during ozonation-filtration reported in previous study [35]. In addition, catalytic ozonation further increased the value of O/C due to stronger oxygenation reaction of •OH than O_3.

COMR treatment decreased the aromaticity of compounds significantly, as described by the decreased value of AI_{mod}. The average DBE value was increased from 8.06 to 8.30, 8.43 and 8.28 during filtration but decreased from 8.06 to 6.67, 6.51 and 4.66 for CMO/CM, CN/CM, and CMO/CN/CM in the presence of O_3, respectively (Fig. S18 and Table S3). Thus, we supposed that the degree of unsaturation of DOM was slightly increased after membrane separation but was significantly decreased after (catalytic) ozonation-filtration. This result is consistent with increasing saturated degree of compounds during AOPs observed in previous studies [30,35]. We also found that catalytic ozonation led to stronger effect on the DBE decrease than ozonation, coincide with other index change. In addition, the relative abundance of O_{2-3} species increased, whereas the relative abundance of O_{4-14} significantly reduced. But we noted that the R_i and DBE of N_1O_2 were still high, due to the presence of $C_{25}H_{36}O_2N_1$ and $C_{37}H_{44}O_2N_1$, which could not be degraded by (catalytic) ozonation. The filtrated water by CMO/CN/CM after catalytic ozonation-filtration showed the highest average value of O/C, and the lowest value of AI_{mod} and DBE among the three catalytic CMs, showing superior catalytic activity.

We did not observe any change in distribution of molecules number of CHO, CHON, CHOS and CHONS during membrane separation. Note that molecules number of CHO increased for catalytic ozonation-filtration due to the slough off of heteroatoms from CHON, CHOS and CHONS by stronger interface catalytic ozonation. The ratio of molecules number of lignins compounds decreased after filtration and oxidation-filtration. We postulate that the lignins compounds were primarily degraded in COMR.

We illustrated similar results as the previous studies that highly unsaturated, aromatic and reduced compounds are preferentially degraded and N-containing compounds possessed the highest reactivity by the reaction of oxidative deamination ($-NH_3 + O_2$) during ozonation process [34,35]. We further demonstrate the superior performance of catalytic ozonation than ozonation that more CHO compounds were mineralized into CO_2 and higher removal of S-containing compounds. Furthermore, our FT-ICR MS observations indicate that the relative intensity and chemical diversity of EfOM exhibit similar change patterns in molecular level among the various catalytic CMs during COMR treatment. This finding highlights the consistency in the performance trends observed across different catalytic systems. Overall, these findings contribute to our understanding of the comparative performance and stability of various catalytic CMs in COMR.

3.3. Complementary function of catalytic ozonation and filtration in the EfOM removal

The molecular properties of compounds by physical separation were obtained through comparing the raw water and water samples treated by filtration without O_3. The removed, produced and resistant compounds were obtained and analyzed through comparing the raw water and water samples treated by COMR for various membranes (Fig. 5 and Fig. S19; details in Table 3). We observed that the physically rejected compounds were enriched in protein and lignin-like compounds with relatively high-oxygen (O/C >0.4) and high M_w (Fig. 5 A). The separation efficiency of CHON, CHOS and CHONS were higher than CHO compounds. Lignin derived compounds accounted for above 65% of the physically rejected compounds. We suppose that physically rejected compounds with higher O/C and heteroatom distribution tends to be treated by COMR.

The removed compounds herein referred to those removed by separation or by oxidation and resistant are refractory compounds. We also observed that removed compounds have higher M_w, DBE and AI_{mod}, but lower H/C and O/C than the resistant compounds, and CHON compounds were the dominant removed compounds (accounting for above 50%) after COMR treatment (Table 3). It has been reported that the large unsaturated compounds with double bonds and activated aromatic rings were preferentially decomposed during ozonation [49]. R_i of CHON class possessed the largest proportion in removed compounds, followed by CHO, CHOS and CHONS classes, both for ozonation and catalytic ozonation (Fig. 5D). Highest reactivity of CHON compounds was explained by easily reactions of ozone or •OH with amines [50,51]. In addition, catalytic ozonation increased the removal of S-containing compounds compared to ozonation. Because CHOS compounds in EfOM were mainly originated from detergents and surface-active substances and sulfonic acids groups of these CHOS compounds could be destroyed by •OH through the cleavage of C-S bond [35]. Therefore, N or S-containing compounds were much easier to be oxidized. And lignin derived and CHO compounds as major components in the secondary effluent primarily contribute to the resistant group compounds.

The produced compounds are those newly formed during (catalytic) ozonation and simultaneously transported across the membrane. Produced compounds have much lower DBE and AI_{mod}, as well as higher O/C and H/C (Table 3), suggesting that the decreased degree of unsaturation in DBE was caused by the breakage of C=C or aliphatic rings instead of C=O of DOM. Reaction of O_3 or hydroxyl radicals with DOM has been reported to produce highly oxidized DOM (O:C>1.0) [52]. But we found that the produced compounds during COMR treatment were not highly oxidized (0.4 <O:C<0.8), which suggests that some highly oxidized DOM will be retained by membrane. Note that CHOS and CHONS were almost not formed in the produced compounds. Thus, we suggested that CHOS and CHONS were transformed to CHO by dominant oxidative desulfonation reactions ($-SH_2$) during (catalytic) ozonation. CHO compounds accounted for 100% of products for the origin CM and most corresponding precursors contained one N atom. However, CHO compounds acted as leading products (58–64%), followed by CHON (35–39%) for catalytic CMs (Table 3). We inferred that the transformation of CHON was dominant by the reaction of oxidative deamination ($-NH_3 + O_2$) during ozonation [34]. However, the transformation of CHON was through the reaction of decyclopropyl ($-C_3H_4$) during catalytic ozonation. In addition, produced compounds after ozonation are more saturated due to the phenolic moieties of EfOM highly reactive with O_3 [53], while they are more oxidated after catalytic ozonation due to the stronger oxygenation reaction of •OH than O_3 [52].

The total number of removed and produced compounds for the origin CM (Fig. 5B) was slightly lower than the catalytic CMs with O_3 (Fig. 5C and Fig. S19), implying that more transformation reactions occurred in the catalytic ozonation than ozonation. Bray-Curtis dissimilarity plots also supported this results. The dissimilarity of all formulae after COMR treatment were much higher than those after filtration treatment and catalytic ozonation further enhanced dissimilarity (Fig. S20A). Dissimilarity of molecular in produced compounds were higher than that in the removed and resistant compound, as illustrated in Fig. S20(B-D).

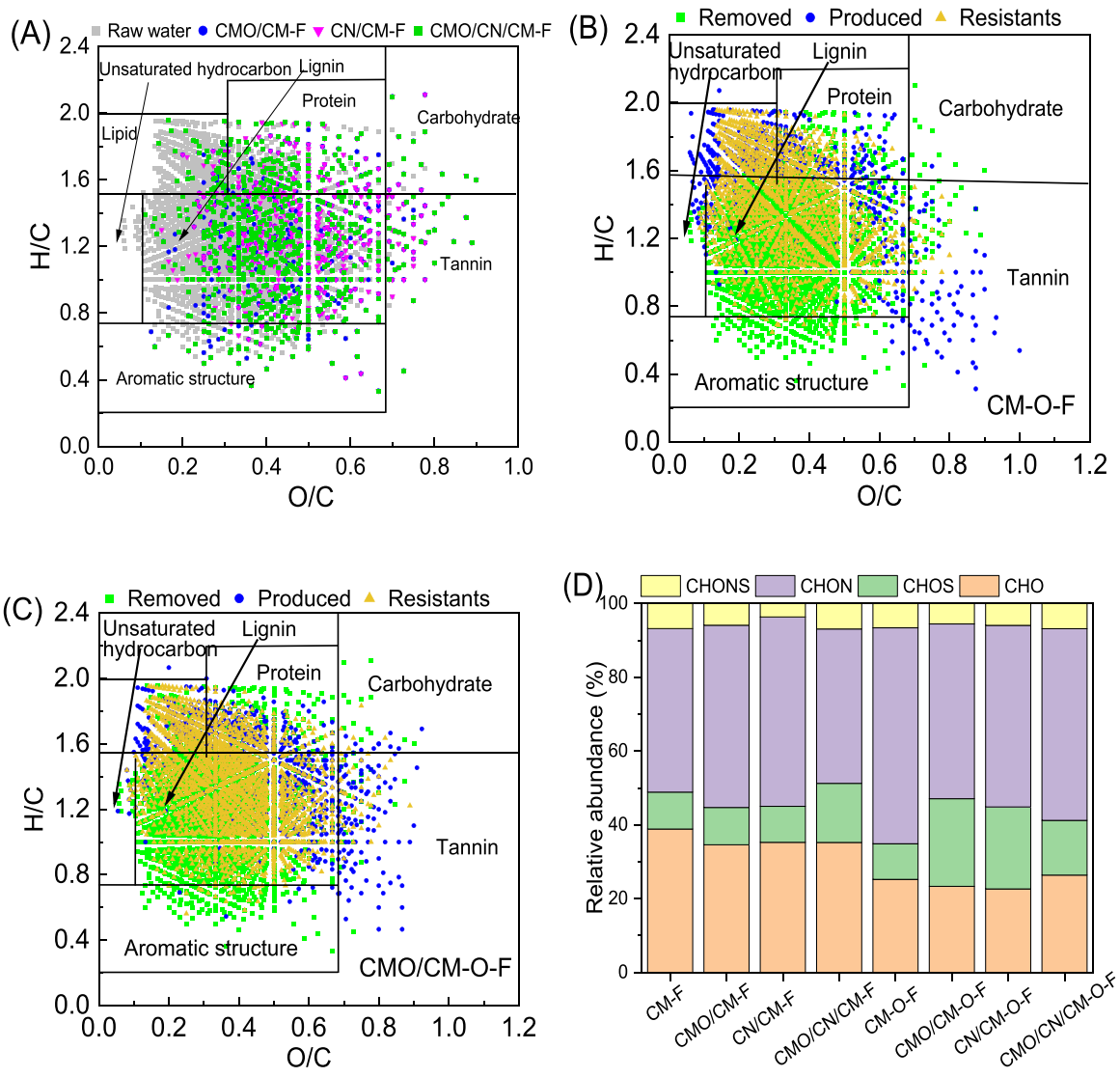

Fig. 5. Van Krevelen diagrams of molecules of physically removed compounds after membrane filtration alone (A), removed, produced and resistant compounds after (catalytic) ozonation-filtration for CM (B) and CMO/CM (C); Relative abundance of four class compounds in removed compounds for filtration and COMR in the presence of 20 mg/L O_3 (D).

Therefore, we propose that catalytic ozonation further enhance the reaction extent of EfOM molecules.

In order to increase the effluent quality of COMR treatment, oxidation capability should be improved towards less aromatic but saturated and oxidated CHO compounds. Additionally, fine ultrafiltration or nanofiltration membrane with strong separation ability are recommended to remove produced compounds formed during oxidation.

3.4. Self-cleaning mechanism analysis in COMR

We conducted physical and chemical cleaning experiments after four cycles of secondary effluent filtration and analyzed membrane fouling resistance after filtration and COMR treatment. As shown in Fig. 6(A), the normalized flux (J/J_0) after four cycles of the secondary effluent filtration was decreased to 15.51%, 26.86%, 16.75%, and 27.41% for CM, CMO/CM, CN/CM and CMO/CN/CM during membrane filtration, respectively, showing no flux recovery after each cycle of filtration. The lower flux decline of coated catalytic CMs than the origin CM without O_3 was attributed to the increase in hydrophilicity (Fig. 7D) [54], where CMO/CM and CMO/CN/CM showed higher anti-fouling performance. Fig. 6(B) presented that the J/J_0 in the presence of O_3 (20 mg/L) showed much lower flux decline than those without O_3. And all tested catalytic CMs showed better flux recovery performance than the origin CM. Thus, the catalytic ozonation-filtration presented stronger self-cleaning property than ozonation-filtration. The J/J_0 of CMO/CN/CM was 92.40%, 92.64%, 90.35% and 91.19% after four cycles of filtration, suggesting the most obvious recovery of flux decline in the presence of O_3 among all the catalytic CMs.

Membrane fouling resistance after filtration of secondary effluent for CM, CMO/CM, CN/CM, and CMO/CN/CM was described in Fig. 6(C). Compared with the origin CM, the catalytic coating slightly decreased the reversible fouling resistance (R_{pr} and R_{cr}) through increasing membrane surface hydrophilicity. The total membrane fouling resistance decreased dramatically, and irreversible fouling resistance (R_{cir}) were completely eliminated after COMR treatment. And the catalytic ozonation presented stronger self-cleaning property than ozonation in COMR. The decrease in fouling resistance was explained by the reaction of foulants with oxidant on the membrane surface. Therefore, catalytic ozonation mitigated membrane fouling and transferred the irreversible fouling to reversible fouling through reducing the total amounts of protein-like materials and soluble microbial byproduct-like materials on the membrane surface (Fig. S21).

Table 3
Molecular characterization of removed, produced and resistant compounds by only filtration and COMR treatment.

	Filtration				COMR											
	CM	CMO/CM	CN/CM	CMO/CN/CM	CM			CMO/CM			CN/ CM			CN/CMO/CM		
	Physically removed compounds				Removed	Produced	Resistant	Removed	Produced	Resistant	Removed	Produced	Resistant	Removed	Produced	Resistant
Lignin (%)	79.01	68.73	66.87	65.54	85.28	21.25	63.64	81.97	35.73	68.99	84.49	30.60	67.87	84.82	32.84	67.74
Protein (%)	6.35	15.80	18.94	16.24	5.99	26.37	12.85	6.77	31.11	14.37	6.78	30.93	14.75	5.68	32.95	14.21
Lipid (%)	6.85	3.20	2.90	5.51	1.45	37.36	21.63	3.84	17.93	13.77	2.06	24.78	14.48	2.23	21.93	15.17
Unsaturated hydrocarbon (%)	0.28	0.00	0.00	0.00	0.55	2.75	0.24	0.33	0.95	0.32	0.40	1.40	0.15	0.32	0.80	0.15
Tannin (%)	1.71	5.12	5.28	3.95	1.32	11.36	1.06	0.91	11.68	1.42	0.74	9.48	1.66	0.82	9.30	1.61
Aromatic structure (%)	5.23	5.76	4.55	7.20	5.02	0.73	0.59	5.73	0.82	0.85	5.09	0.65	0.77	5.68	0.57	0.81
Carbohydrate (%)	0.56	1.39	1.45	1.55	0.38	0.18	0.00	0.46	1.77	0.28	0.44	2.16	0.31	0.46	1.61	0.31
High M_w (%)	43.89	52.78	54.00	53.54	42.23	49.45	43.60	39.40	49.54	38.99	39.42	52.63	38.99	40.74	53.12	37.66
Med M_w (%)	34.22	27.24	29.92	30.93	38.06	29.01	33.71	39.97	31.27	37.13	40.29	28.54	36.89	38.60	29.13	38.85
Low M_w (%)	21.88	19.98	16.09	15.53	19.70	21.53	22.69	20.63	19.19	23.88	20.29	18.83	24.11	20.67	17.74	23.49
Avg M_w (Da)	390.27	412.99	416.17	415.17	416.82	399.63	384.91	382.38	401.55	376.65	382.34	409.83	377	384.51	410.88	375.10
O/C	0.35	0.45	0.46	0.43	0.38	0.39	0.34	0.34	0.47	0.37	0.34	0.44	0.37	0.33	0.45	0.38
H/C	1.17	1.24	1.27	1.24	1.29	1.48	1.38	1.18	1.45	1.34	1.16	1.50	1.35	1.15	1.49	1.34
Al_{mod}	0.37	0.27	0.25	0.28	0.25	0.15	0.23	0.37	0.14	0.26	0.38	0.12	0.25	0.39	0.12	0.25
NOSC	-0.27	-0.17	-0.18	-0.20	-0.39	-0.70	-0.71	-0.29	-0.38	-0.51	-0.27	-0.51	-0.52	-0.27	-0.46	-0.50
DBE		8.28	8.03	8.42	8.26	5.57	6.71	8.96	5.90	6.91	9.12	5.58	6.84	9.23	5.67	6.87
8.97																
CHO (%)		31.41	32.89	31.21	21.12	100	100	21.24	62.81	70.60	19.83	63.66	69.59	21.51	58.16	64.92
32.08																
CHON (%)		48.93	51.33	45.35	54.98	0	0	49.35	35.87	29.36	50.00	35.12	29.68	49.82	39.21	31.06
44.73																
CHOS (%)		10.58	9.22	13.18	12.58	0	0	18.73	1.31	0.04	19.00	1.21	0.72	16.84	2.63	4.02
12.71																
CHONS (%)		9.08	6.56	10.26	11.33	0	0	10.68	0.00	0.00	11.17	0.00	0.00	11.82	0.00	0.00
10.48																

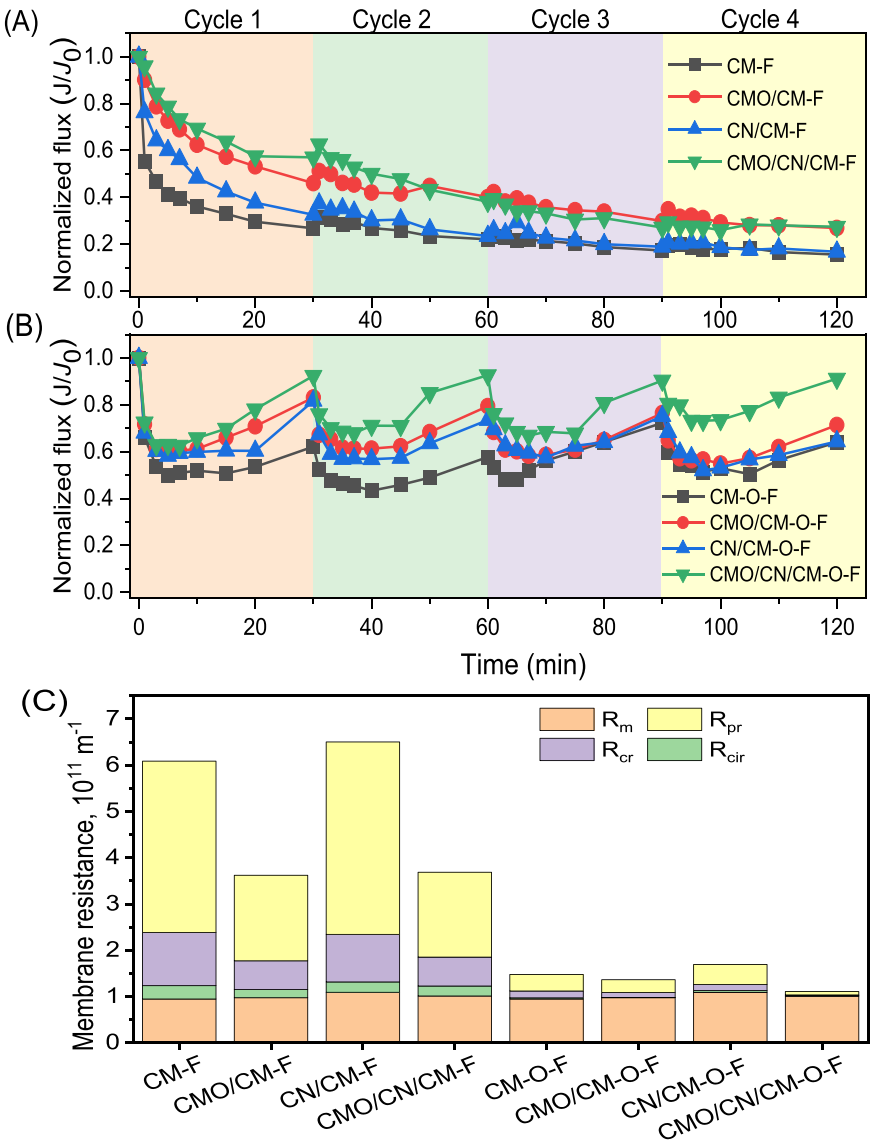

Fig. 6. Normalized flux during filtration of four cycles without O_3 (A) and with 20 mg/L O_3 (B) and membrane fouling resistance analysis (C) for CM, CMO/CM, CN/CM, and CMO/CN/CM.

After adding O_3, the thickness of the fouling layer for the origin CM was slightly decreased but it dramatically decreased to less than 10 μm for catalytic CMs after COMR treatment (Fig. 7A). And the mean pores size of the fouling layer also increased dramatically for CMO/CN/CM in the presence of O_3 (Fig. 7B). The SEM images showed a relatively porous and loose fouling layer with obvious cracks for CMO/CM and CMO/CN/CM in the presence of O_3 (Fig. S22 and Fig. S23). Therefore, we suppose that catalytic ozonation effectively removed foulants on the membrane surface and caused the thin, porous and loose fouling layer formation, which could be flushed away more easily by physical cleaning [55]. Catalytic coating increased the surface roughness and foulants accumulation further increased the roughness during filtration. However, the macromolecular are decomposed into small molecules during (catalytic) ozonation, which filled the valleys and made the surface smooth (Fig. 7C). The hydrophilicity of fouled catalytic CMs were similar with the clean catalytic CMs in the presence of O_3 and catalytic ozonation led to higher membrane hydrophilicity than ozonation (Fig. 7D), which could be attributed to the strong self-cleaning property during catalytic ozonation.

PCA and Spearman correlations between the fouling indexes and the molecular-level parameters of removed EfOM were performed. Samples from filtration and COMR treatment distributed separately and shared few similarities. Higher hydrophilicity of the membrane surface after COMR treatment could be explained by the molecular-level parameter of O/C and H/C (Fig. S24A). Fouling resistance showed strong positive correlation with molecular-level parameter of O/C but negative correlation with DBE and Al_{mod} of removed compounds (Fig. S24B). The higher flux of CMO/CN/CM after four cycles of filtration in the presence of O_3 was explained by the superior catalytic activity at molecular level. Relative abundance of CHO (Ra_{CHO}) showed strong positive correlation with membrane fouling resistance. Thus, mineralization of EfOM by catalytic ozonation explained decreased membrane fouling.

4. Conclusions

In this study, we systematically investigated the impacts of catalytic ozonation on the molecular-level transformation of EfOM and self-cleaning mechanism in COMR. Firstly, the complementary function of catalytic ozonation and filtration in the EfOM removal were confirmed. The filtration mainly removed protein-like materials, which are enriched in relatively high-oxygen compounds (O/C >0.4) with high molecular weight. Catalytic ozonation further removed humic-like

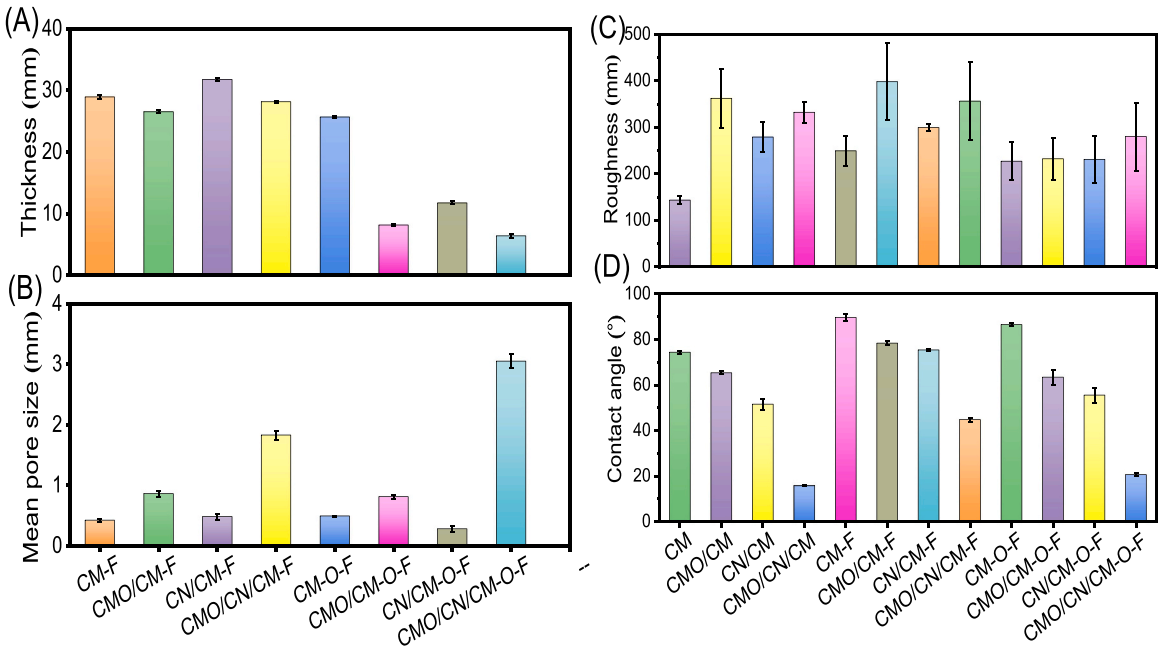

Fig. 7. Clean and fouled catalytic membranes characterization: surface pore size (A), fouling layer thickness (B), roughness (C) and hydrophilicity (D).

materials and highly unsaturated, aromatic and reduced compounds (O/C<0.4; H/C<1.3), producing oxidated and saturated compounds. It is supposed that physically rejected compounds with higher oxygen and heteroatom tends to be treated by catalytic ozonation and oxidized compounds tends to be retained by membrane filtration. Residual organics risk in the effluent of COMR imply that oxidation capacity and membrane separation ability need to be matched properly in oxidation-filtration process.

Additionally, molecular-level evidence for the superior performance of catalytic ozonation was delineated. We demonstrate that catalytic ozonation-filtration led to preferential removal of medium molecular weighted microbial humic-like materials and S-containing compounds, enhancing the reaction extent of EfOM molecules and causing higher mineralization, compared to ozonation-filtration. Produced compounds after ozonation are more saturated due to the phenolic moieties of EfOM highly reactive with O_3, while they are more oxidated after catalytic ozonation due to the stronger oxygenation reaction of •OH than O_3.

Catalytic ozonation transferred the irreversible fouling to reversible fouling and exhibited strong self-cleaning property, which could be explained by superior performance on EfOM removal and the characteristics of fouling layers.

CRediT authorship contribution statement

Chen Li: Conceptualization, Methodology, Software. **Zhenbei Wang**: Data curation, Formal analysis. **Ao Li**: Writing – original draft. **Zilong Song**: Visualization, Investigation. **Ruijun Ren**: Software, Validation. **Kuichang Zuo:** Writing – review & editing. **Fei Qi:** Supervision, Funding acquisition. **Amir Ikhlaq:** Writing – review & editing. **Oksana Ismailova:** Software, Validation.

Declaration of Competing Interest

The authors declare that they have no known competing financial interests or personal relationships that could have appeared to influence the work reported in this paper.

Data Availability

No data was used for the research described in the article.

Acknowledgments

We thank the Large-scale Instrument Innovation Fund of Beijing Forestry University (BJFU-DXYQCX-2022–01), the National Key Research and Development Program of China (2021YFE0100800), the National Natural Science Foundation of China (Nos. 51878047, 22076012, 52100002 and 52200035), the Beijing Forestry University Outstanding Young Talent Cultivation Project (No. 2019JQ03008) and China Postdoctoral Science Foundation (2021M700448) for funding supporting.

Appendix A. Supporting information

Supplementary data associated with this article can be found in the online version at doi:10.1016/j.apcatb.2023.123076.

References

[1] H. Cheng, Y. Hu, J. Zhao, Meeting China's water shortage crisis: current practices and challenges, Environ. Sci. Technol. 43 (2009) 240–244, https://doi.org/10.1021/es801934a.
[2] I. Michael-Kordatou, C. Michael, X. Duan, X. He, D.D. Dionysiou, M.A. Mills, D. Fatta-Kassinos, Dissolved effluent organic matter: Characteristics and potential implications in wastewater treatment and reuse applications, Water Res. 77 (2015) 213–248, https://doi.org/10.1016/j.watres.2015.03.011.
[3] E. Jennings, A. Kremser, L. Han, T. Reemtsma, O.J. Lechtenfeld, Discovery of polar ozonation byproducts via direct injection of effluent organic matter with online LC-FT-ICR-MS, Environ. Sci. Technol. 56 (2022) 1894–1904, https://doi.org/10.1021/acs.est.1c04310.
[4] X. Luo, S. Yu, D. Xu, J. Ding, X. Zhu, J. Xing, T. Wu, X. Zheng, T.M. Aminabhavi, X. Cheng, H. Liang, Isoporous catalytic ceramic membranes for ultrafast contaminants elimination through boosting confined radicals, Chem. Eng. J. 455 (2023), 140872, https://doi.org/10.1016/j.cej.2022.140872.
[5] M.B. Asif, Z. Zhang, Ceramic membrane technology for water and wastewater treatment: a critical review of performance, full-scale applications, membrane fouling and prospects, Chem. Eng. J. 418 (2021), 129481, https://doi.org/10.1016/j.cej.2021.129481.
[6] Z. Song, J. Sun, W. Wang, Z. Wang, Y. Zhang, B. Xu, F. Qi, Stable synergistic decontamination and self-cleaning performance of powerful N-rGO catalytic ozonation membrane: clustering effect of free electrons and role of interface properties, Appl. Catal. B Environ. 283 (2021), 119662, https://doi.org/10.1016/j.apcatb.2020.119662.
[7] B.I. Harman, H. Koseoglu, N.O. Yigit, M. Beyhan, M. Kitis, The use of iron oxide-coated ceramic membranes in removing natural organic matter and phenol from waters, Desalination 261 (2010) 27–33, https://doi.org/10.1016/j.desal.2010.05.052.

[8] S. Byun, S.H. Davies, A.L. Alpatova, L.M. Corneal, M.J. Baumann, V.V. Tarabara, S. J. Masten, Mn oxide coated catalytic membranes for a hybrid ozonation–membrane filtration: comparison of Ti, Fe and Mn oxide coated membranes for water quality, Water Res. 45 (2011) 163–170, https://doi.org/10.1016/j.watres.2010.08.031.
[9] Y.X. Hu, N. Milne, S. Gray, G. Morris, W.Q. Jin, M. Duke, B. Zhu, Combined TiO_2 membrane filtration and ozonation for efficient water treatment to enhance the reuse of wastewater, Desalin. Water Treat. 34 (2011) 57–62, https://doi.org/10.5004/dwt.2011.2867.
[10] S. Zhan, H. Huang, C. He, Y. Xiong, P. Li, S. Tian, Controllable synthesis of substitutional and interstitial nitrogen-doped ceria: The effects of doping sites on enhanced catalytic ozonation of organic pollutants, Appl. Catal. B Environ. 321 (2023), 122040, https://doi.org/10.1016/j.apcatb.2022.122040.
[11] Y. Guo, Z.L. Song, B.B. Xu, Y.N. Li, F. Qi, J.P. Croue, D.H. Yuan, A novel catalytic ceramic membrane fabricated with $CuMn_2O_4$ particles for emerging UV absorbers degradation from aqueous and membrane fouling elimination, J. Hazard. Mater. 344 (2018) 1229–1239, https://doi.org/10.1016/j.jhazmat.2017.11.044.
[12] A. Li, Y. Liu, Z. Wang, Z. Song, Y. Zhang, Y. Wang, B. Xu, F. Qi, A. Ikhlaq, J. Kumirska, E. Maria Siedlecka, Catalytic ozonation membrane reactor integrated with $CuMn_2O_4$/rGO for degradation emerging UV absorbers (BP-4) and fouling in-situ self-cleaning, Sep. Purif. Technol. 279 (2021), 119804, https://doi.org/10.1016/j.seppur.2021.119804.
[13] J. Zhang, B. Xin, C. Shan, W. Zhang, D.D. Dionysiou, B. Pan, Roles of oxygen-containing functional groups of O-doped g-C_3N_4 in catalytic ozonation: quantitative relationship and first-principles investigation, Appl. Catal. B Environ. 292 (2021), 120155, https://doi.org/10.1016/j.apcatb.2021.120155.
[14] Y. Liu, Z. Song, W. Wang, Z. Wang, Y. Zhang, C. Liu, Y. Wang, A. Li, B. Xu, F. Qi, A $CuMn_2O_4$/g-C_3N_4 catalytic ozonation membrane reactor used for water purification: membrane fabrication and performance evaluation, Sep. Purif. Technol. 265 (2021), 118268, https://doi.org/10.1016/j.seppur.2020.118268.
[15] C. Mansas, J. Mendret, S. Brosillon, A. Ayral, Coupling catalytic ozonation and membrane separation: a review, Sep. Purif. Technol. 236 (2020), https://doi.org/10.1016/j.seppur.2019.116221.
[16] C. Li, W. Sun, Z. Lu, X. Ao, S. Li, Ceramic nanocomposite membranes and membrane fouling: a review, Water Res. 175 (2020), 115674, https://doi.org/10.1016/j.watres.2020.115674.
[17] C. Mansas, J. Mendret, S. Brosillon, A. Ayral, Coupling catalytic ozonation and membrane separation: a review, Sep. Purif. Technol. 236 (2020), 116221, https://doi.org/10.1016/j.seppur.2019.116221.
[18] R. Chen, K. Zhang, H. Wang, X.-m Wang, X.-h Zhang, X. Huang, Incorporating catalytic ceramic membrane into the integrated process of in situ ozonation, membrane filtration and biological degradation: enhanced performance and underlying mechanisms, J. Membr. Sci. 652 (2022), 120509, https://doi.org/10.1016/j.memsci.2022.120509.
[19] X. Yang, F.L. Rosario-Ortiz, Y. Lei, Y. Pan, X. Lei, P. Westerhoff, Multiple roles of dissolved organic matter in advanced oxidation processes, Environ. Sci. Technol. 56 (2022) 11111–11131, https://doi.org/10.1021/acs.est.2c01017.
[20] Z. Chen, M. Li, Q. Wen, N. Ren, Evolution of molecular weight and fluorescence of effluent organic matter (EfOM) during oxidation processes revealed by advanced spectrographic and chromatographic tools, Water Res. 124 (2017) 566–575, https://doi.org/10.1016/j.watres.2017.08.006.
[21] C. Li, W. Sun, Z. Lu, X. Ao, S. Li, Z. Wang, F. Qi, O. Ismailova, Contribution of filtration and photocatalysis to DOM removal and fouling mechanism during in-situ UV-LED photocatalytic ceramic membrane process, Water Res. 226 (2022), 119298, https://doi.org/10.1016/j.watres.2022.119298.
[22] F. Hammes, E. Salhi, O. Köster, H.P. Kaiser, T. Egli, U. von Gunten, Mechanistic and kinetic evaluation of organic disinfection by-product and assimilable organic carbon (AOC) formation during the ozonation of drinking water, Water Res. 40 (2006) 2275–2286, https://doi.org/10.1016/j.watres.2006.04.029.
[23] Z. Song, Y. Li, Z. Wang, J. Sun, X. Xu, Z. Huangfu, C. Li, Y. Zhang, B. Xu, F. Qi, A. Ikhlaq, J. Kumirska, E.M. Siedlecka, Interfacial reactions of catalytic ozone membranes resulting in the release and degradation of irreversible foulants, Water Res. 226 (2022), 119244, https://doi.org/10.1016/j.watres.2022.119244.
[24] S. Saeid, P. Tolvanen, N. Kumar, K. Eränen, J. Peltonen, M. Peurla, J.-P. Mikkola, A. Franz, T. Salmi, Advanced oxidation process for the removal of ibuprofen from aqueous solution: a non-catalytic and catalytic ozonation study in a semi-batch reactor, Appl. Catal. B Environ. 230 (2018) 77–90, https://doi.org/10.1016/j.apcatb.2018.02.021.
[25] B. Kasprzyk-Hordern, U. Raczyk-Stanisławiak, J. Świetlik, J. Nawrocki, Catalytic ozonation of natural organic matter on alumina, Appl. Catal. B Environ. 62 (2006) 345–358, https://doi.org/10.1016/j.apcatb.2005.09.002.
[26] X. Jin, W. Zhang, R. Hou, P. Jin, J. Song, X.C. Wang, Tracking the reactivity of ozonation towards effluent organic matters from WWTP using two-dimensional correlation spectra, J. Environ. Sci. (China) 76 (2019) 289–298, https://doi.org/10.1016/j.jes.2018.05.012.
[27] J. Kim, W. Shan, S.H.R. Davies, M.J. Baumann, S.J. Masten, V.V. Tarabara, Interactions of aqueous NOM with nanoscale TiO_2: implications for ceramic membrane filtration-ozonation hybrid process, Environ. Sci. Technol. 43 (2009) 5488–5494, https://doi.org/10.1021/es900342q.
[28] W. Bahureksa, M.M. Tfaily, R.M. Boiteau, R.B. Young, M.N. Logan, A.M. McKenna, T. Borch, Soil organic matter characterization by fourier transform ion cyclotron resonance mass spectrometry (FTICR MS): a critical review of sample preparation, analysis, and data interpretation, Environ. Sci. Technol. 55 (2021) 9637–9656, https://doi.org/10.1021/acs.est.1c01135.
[29] Y. Sun, X. Li, X. Li, J. Wang, Deciphering the fingerprint of dissolved organic matter in the soil amended with biodegradable and conventional microplastics based on optical and molecular signatures, Environ. Sci. Technol. 56 (2022) 15746–15759, https://doi.org/10.1021/acs.est.2c06258.
[30] B. Zhang, X. Wang, Z. Fang, S. Wang, C. Shan, S. Wei, B. Pan, Unravelling molecular transformation of dissolved effluent organic matter in UV/H_2O_2, UV/persulfate, and UV/chlorine processes based on FT-ICR-MS analysis, Water Res. 199 (2021), 117158, https://doi.org/10.1016/j.watres.2021.117158.
[31] Y. Wang, Y. Xiang, M. Marques dos Santos, G. Wei, B. Jiang, S. Snyder, C. Shang, J.-P. Croué, UV/chlorine and chlorination of effluent organic matter fractions: Tracing nitrogenous DBPs using FT-ICR mass spectrometry, Water Res. 231 (2023), 119646, https://doi.org/10.1016/j.watres.2023.119646.
[32] P. Du, W. Liu, Q. Zhang, P. Zhang, C. He, Q. Shi, C.-H. Huang, J. Wang, Transformation of dissolved organic matter during UV/peracetic acid treatment, Water Res. (2023), 119676, https://doi.org/10.1016/j.watres.2023.119676.
[33] P. Phungsai, F. Kurisu, I. Kasuga, H. Furumai, Molecular characterization of low molecular weight dissolved organic matter in water reclamation processes using Orbitrap mass spectrometry, Water Res. 100 (2016) 526–536, https://doi.org/10.1016/j.watres.2016.05.047.
[34] Z. Song, Z. Wang, J. Ma, J. Sun, C. Li, X. Xu, C. Chen, Z. Chen, B. Xu, Y. Jiang, J. Kumirska, E.M. Siedlecka, A. Ikhlaq, F. Qi, O. Ismailova, Molecular levels unveil the membrane fouling mitigation mechanism of a superpotent N-rGO catalytic ozonation membrane: Interfacial catalytic reaction pathway and induced EfOM transformation reactions, Appl. Catal. B Environ. 319 (2022), 121943, https://doi.org/10.1016/j.apcatb.2022.121943.
[35] B. Zhang, C. Shan, S. Wang, Z. Fang, B. Pan, Unveiling the transformation of dissolved organic matter during ozonation of municipal secondary effluent based on FT-ICR-MS and spectral analysis, Water Res. 188 (2021), 116484, https://doi.org/10.1016/j.watres.2020.116484.
[36] T. Maqbool, M. Sun, L. Chen, Z. Zhang, Exploring the fate of dissolved organic matter at the molecular level in the reactive electrochemical ceramic membrane system using fluorescence spectroscopy and FT-ICR MS, Water Res. 210 (2022), 117979, https://doi.org/10.1016/j.watres.2021.117979.
[37] C.-X. Geng, N. Cao, W. Xu, C. He, Z.-W. Yuan, J.-W. Liu, Q. Shi, C.-M. Xu, S.-T. Liu, H.-Z. Zhao, Molecular characterization of organics removed by a covalently bound inorganic–organic hybrid coagulant for advanced treatment of municipal sewage, Environ. Sci. Technol. 52 (2018) 12642–12648, https://doi.org/10.1021/acs.est.8b03306.
[38] D.D. Phong, J. Hur, Non-catalytic and catalytic degradation of effluent dissolved organic matter under UVA-and UVC-irradiation tracked by advanced spectroscopic tools, Water Res. 105 (2016) 199–208, https://doi.org/10.1016/j.watres.2016.08.068.
[39] C.A. Stedmon, R. Bro, Characterizing dissolved organic matter fluorescence with parallel factor analysis: a tutorial, Limnol. Oceanogr. Methods 6 (2008) 572–579, https://doi.org/10.4319/lom.2008.6.572b.
[40] X. Wang, W. Schrader, Selective analysis of sulfur-containing species in a heavy crude oil by deuterium labeling reactions and ultrahigh resolution mass spectrometry, Int. J. Mol. Sci. 16 (2015) 30133–30143, https://doi.org/10.3390/ijms161226205.
[41] M.-H. Lee, Y.K. Lee, M. Derrien, K. Choi, K.H. Shin, K.-S. Jang, J. Hur, Evaluating the contributions of different organic matter sources to urban river water during a storm event via optical indices and molecular composition, Water Res. 165 (2019), 115006, https://doi.org/10.1016/j.watres.2019.115006.
[42] T. Zhang, J. Lu, J. Ma, Z. Qiang, Comparative study of ozonation and synthetic goethite-catalyzed ozonation of individual NOM fractions isolated and fractionated from a filtered river water, Water Res. 42 (2008) 1563–1570, https://doi.org/10.1016/j.watres.2007.11.005.
[43] D. Wei, Y. Tao, Z. Zhang, X. Zhang, Effect of pre-ozonation on mitigation of ceramic UF membrane fouling caused by algal extracellular organic matters, Chem. Eng. J. 294 (2016) 157–166, https://doi.org/10.1016/j.cej.2016.02.110.
[44] X. Jin, S. Peldszus, P.M. Huck, Reaction kinetics of selected micropollutants in ozonation and advanced oxidation processes, Water Res. 46 (2012) 6519–6530, https://doi.org/10.1016/j.watres.2012.09.026.
[45] P. Jin, X. Jin, V.A. Bjerkelund, S.W. Østerhus, X.C. Wang, L. Yang, A study on the reactivity characteristics of dissolved effluent organic matter (EfOM) from municipal wastewater treatment plant during ozonation, Water Res. 88 (2016) 643–652, https://doi.org/10.1016/j.watres.2015.10.060.
[46] S.S. Yekta, M. Gonsior, P. Schmitt-Kopplin, B.H. Svensson, Characterization of dissolved organic matter in full scale continuous stirred tank biogas reactors using ultrahigh resolution mass spectrometry: a qualitative overview, Environ. Sci. Technol. 46 (2012) 12711–12719, https://doi.org/10.1021/es3024447.
[47] Y. Shi, S. Li, L. Wang, Q. Yu, G. Shen, J. Li, K. Xu, H. Ren, J. Geng, Compositional characteristics of dissolved organic matter in pharmaceutical wastewater effluent during ozonation, Sci. Total Environ. 778 (2021), 146278, https://doi.org/10.1016/j.scitotenv.2021.146278.
[48] W. Chen, C. He, Z. Gu, F. Wang, Q. Li, Molecular-level insights into the transformation mechanism for refractory organics in landfill leachate when using a combined semi-aerobic aged refuse biofilter and chemical oxidation process, Sci. Total Environ. 741 (2020), 140502, https://doi.org/10.1016/j.scitotenv.2020.140502.
[49] S. Lim, J.L. Shi, U. von Gunten, D.L. McCurry, Ozonation of organic compounds in water and wastewater: a critical review, Water Res. 213 (2022), 118053, https://doi.org/10.1016/j.watres.2022.118053.
[50] S. Merel, S. Lege, J.E. Yanez Heras, C. Zwiener, Assessment of N-oxide formation during wastewater ozonation, Environ. Sci. Technol. 51 (2017) 410–417, https://doi.org/10.1021/acs.est.6b02373.
[51] M. Yasuda, T. Tomo, S. Hirata, T. Shiragami, T. Matsumoto, Neighboring hetero-atom assistance of sacrificial amines to hydrogen evolution using Pt-loaded TiO_2-

photocatalyst, Catalysts 4 (2014) 162–173, https://doi.org/10.3390/catal4020162.
[52] C.K. Remucal, E. Salhi, N. Walpen, U. von Gunten, Molecular-level transformation of dissolved organic matter during oxidation by ozone and hydroxyl radical, Environ. Sci. Technol. 54 (2020) 10351–10360, https://doi.org/10.1021/acs.est.0c03052.
[53] M.K. Ramseier, U. von Gunten, Mechanisms of phenol ozonation-kinetics of formation of primary and secondary reaction products, Ozone Sci. Eng. 31 (2009) 201–215, https://doi.org/10.1080/01919510902740477.
[54] C. Li, W. Sun, Z. Lu, X. Ao, C. Yang, S. Li, Systematic evaluation of TiO_2-GO-modified ceramic membranes for water treatment: Retention properties and fouling mechanisms, Chem. Eng. J. 378 (2019), 122138, https://doi.org/10.1016/j.cej.2019.122138.
[55] Z. Song, Y. Li, Z. Wang, M. Wang, Z. Wang, Y. Zhang, J. Sun, C. Liu, Y. Liu, B. Xu, F. Qi, Effect of the coupling modes on EfOM degradation and fouling mitigation in ozonation-ceramic membrane filtration, Chem. Eng. J. 394 (2020), 124935, https://doi.org/10.1016/j.cej.2020.124935.